JOC The Journal of Organic Chemistry

Article

pubs.acs.org/joc

Mechanism of Rhodium-Catalyzed Formyl Activation: A Computational Study

Xiaoling Luo,[†,§] Ruopeng Bai,[‡,§] Song Liu,[†] Chunhui Shan,[†] Changguo Chen,[*,†] and Yu Lan[*,†]

[†]School of Chemistry and Chemical Engineering, Chongqing University, Chongqing 400030, People's Republic of China

[‡]College of Chemistry and Molecular Sciences, Wuhan University, Wuhan, Hubei 430072, People's Republic of China

Supporting Information

ABSTRACT: Metal-catalyzed transfer hydroformylation is an important way of cleaving C−C bonds and constructing new double bonds. The newly reported density functional theory (DFT) method, M11-L, has been used to clarify the mechanism of the rhodium-catalyzed transfer hydroformylation reported by Dong et al. DFT calculations depict a deformylation and formylation reaction pathway. The deformylation step involves an oxidative addition to the formyl C−H bond, deprotonation with a counterion, decarbonylation, and β-hydride elimination. After olefin exchange, the formylation step takes place via olefin insertion into the Rh−H bond, carbonyl insertion, and a final protonation with the conjugate acid of the counterion. Theoretical calculations indicate that the alkalinity of the counterion is important for this reaction because both deprotonation and protonation occur during the catalytic cycle. A theoretical study into the formyl acceptor shows that the driving force of the reaction is correlated with the stability of the unsaturated bond in the acceptor. Our computational results suggest that alkynes or ring-strained olefins could be used as formyl acceptors in this reaction.

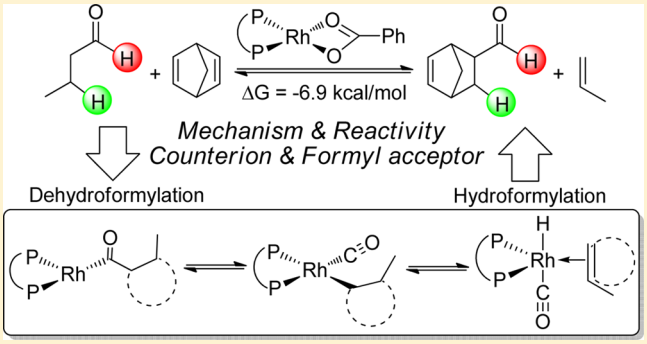

INTRODUCTION

C−C bond cleavage reactions are widely used for the modifications of organic frameworks and, thus, have received much attention by researchers in the past several decades.[1] As an example, dehydroformylation reactions have recently become a hot topic for the new realization of C−C bond cleavage.[2] This conversion was first observed in 2007 by Waterman, who found lanosterol demethylase converting aldehydes to olefins by dehydroformylation.[3] Indeed, this conversion widely exists during the biosynthesis of sterols in bacteria, algae, fungi, plants, and animals, which are catalyzed by sterol demethylase.[4] Homogeneously catalyzed hydroformylation, the reverse reaction of dehydroformylation, has been extensively explored by experimental[5] and computational studies[6] over recent decades to provide useful strategies for the conversion of olefins to aldehydes. However, few reports concern homogeneous dehydroformylation, as it was previously considered to be a thermodynamically disfavored process.[7]

In dehydroformylation, one molecule of carbon monoxide (CO) and one molecule of hydrogen (H_2) are formally removed from an aldehyde, with concomitant olefin formation. To overcome this thermodynamically unfavorable process, dehydroformylation is designed as a formyl transfer procedure, whereby the aldehyde is the source of CO and H_2, which are absorbed by the olefin reagent. Formyl transfer was first observed as a side reaction of decarbonylation reactions in 1990 by Watanabe et al.[8] Formyl transfer from heptanal to cyclohexene took place in their reported intermolecular hydroacylation to afford cyclohexanal as a side product. In this transhydroformylation, a typical reaction was carried out at 200 °C, under 20 atm of CO, with $Ru_3(CO)_{12}$ as catalyst, to give only 29% yield of cyclohexanal. Therefore, there is a requirement to find mild conditions for homogeneously catalyzed dehydroformylation reactions to achieve a robust synthetic method.

Recently, Dong et al.[9] reported rhodium-catalyzed dehydroformylation (Scheme 1), which represented a powerful method for formyl transfer under mild conditions, leading to an efficient synthesis of olefins with high yields (up to 99%) and chemoselectivity (>99:1). In this reaction, strained olefin norbornadiene (nbd) acted as a formyl acceptor in the concomitant dehydroformylation, thus avoiding the accumulation of CO gas, which acts as a catalyst poison in the aldehyde

Scheme 1. Rh-Catalyzed C−C Bond Cleavage by Transfer Hydroformylation

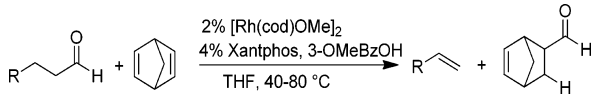

Received: December 14, 2015
Published: February 24, 2016

DOI: 10.1021/acs.joc.5b02828
J. Org. Chem. 2016, 81, 2320−2326

activation. Release of ring strain in the olefin[10] is the driving force for this type of reaction, which leads to the formation of strain-free olefin products.[11]

Mechanistically, formyl activation is the key step of this rhodium-catalyzed transfer hydroformylation.[12] As shown in Scheme 2, there are generally three possible pathways for this step: Pathway 1 proceeds through formyl C−H bond cleavage followed by carbonyl elimination to afford a carbonyl metal−hydride complex. In contrast, direct formyl oxidative addition in pathway 2 or β-hydride oxidative addition followed by formyl elimination in pathway 3 is also possible. Here, we describe the use of density functional theory (DFT) calculations to investigate the mechanism of this rhodium-catalyzed transfer hydroformylation. Counterion effects and the reactivity of strained olefins are also considered theoretically.

Scheme 2. Possible Modes for Formyl Activation

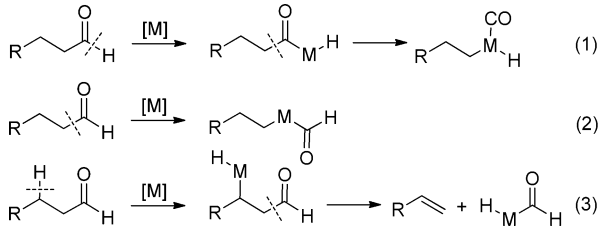

COMPUTATIONAL METHODS

All of the DFT calculations conducted in this study were carried out using the Gaussian 09 series of programs.[13] Density functional M11-L, proposed by Truhlar et al.,[14] with a standard 6-31G(d) basis set (SDD[15] basis set for Rh), was used for the geometry optimizations. Harmonic vibrational frequency calculations were performed for all stationary points to confirm them as local minima or transition structures and to derive the thermochemical corrections for the enthalpies and free energies. The same DFT method was used with a 6-311+G(d,p) basis set (LanL08-f[16] basis set for Rh) to calculate the single-point energies. Solvent effects were taken into consideration using single-point calculations based on the gas-phase stationary points with a SMD[17] continuum solvation model. The energies presented in this paper are the M11-L/6-311+G(d,p) calculated Gibbs free energies in THF, with M11-L/6-31G(d) calculated thermodynamic corrections. As a comparison, some other density functionals, such as M06-L, M06-2X, and TPSS, were also employed to calculate the main catalytic cycle (Figure S1 in Supporting Information). The same trend of the free energy profiles was found with those methods. Therefore, the current M11-L method used in our work is reliable. We also tried to use the M11-L/6-311+G(d,p) method and basis set to optimize the geometry and calculated the single-point energy with the same method and basis set. The computational results (Figure S2 in Supporting Information) were much closer to the reported data in the current work. Furthermore, the accurate combinational CBS-QB3 method was employed as a free energy standard to evaluate the density functional M11-L. The observed free energy difference of reaction energy is only 0.5 kcal/mol between those two methods (Table S1 in Supporting Information); therefore, M11-L is reliable in the current work.

RESULTS AND DISCUSSION

The general mechanisms for rhodium-catalyzed transfer hydroformylation are shown in Scheme 3. The process begins with ligand-coordinated rhodium acetate complex **A**. Oxidative addition[18] of a formyl C−H bond followed by deprotonation generates acylrhodium intermediate **B**. Subsequent decarbonylation and β-hydride elimination via intermediate **C** forms olefin-coordinated carbonyl rhodium hydride intermediate **D**.

Scheme 3. Possible Reaction Pathways for Rhodium-Catalyzed Transfer Hydroformylation

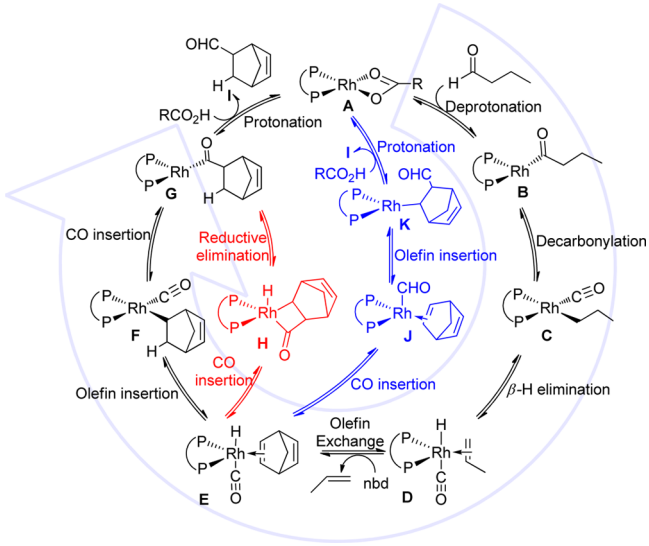

After olefin exchange with nbd, nbd-coordinated rhodium complex **E** is generated, which is a common intermediate for subsequent reaction pathways. Olefin insertion into the Rh−H bond generates intermediate **F**, and acylrhodium species **G** is formed by carbonyl insertion. The protonation of intermediate **G** produces aldehyde **I**, and active catalyst **A** is regenerated. Alternatively, acylrhodium **G** could also be generated by carbonyl insertion and reductive elimination via intermediate **H**. In another pathway, carbonyl insertion into the Rh−H bond in intermediate **E** forms acylrhodium intermediate **J**. An nbd insertion then affords intermediate **K**, which is protonated to yield the same aldehyde **I**. With the proposed pathways in hand, DFT calculations were performed to reveal the mechanism of this rhodium-catalyzed transfer hydroformylation.

In the experiment, nbd is the best formyl acceptor for the transfer hydroformylation. As shown in Figure 1, we initially investigated the mechanism of the rhodium-catalyzed transfer hydroformylation between butyraldehyde and nbd (reaction 4). The free energy profiles for the initial steps of this rhodium-catalyzed transfer hydroformylation are shown in Figure 2.

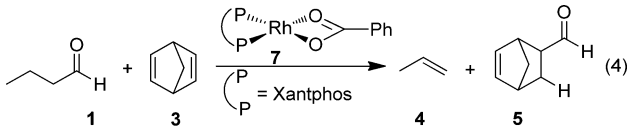

Figure 1. Rhodium-catalyzed transfer hydroformylation of butyraldehyde and nbd, the model reaction for the theoretical study.

Rhodium benzoate complex **7** was set to a relative zero value and was generated from the $[Rh(cod)OMe]_2$ catalyst through dissociation and ligand exchange reactions in the presence of benzoic acid and Xantphos. Coordination of butyraldehyde to the catalyst led to intermediate **8** in an endothermic process, which was mainly attributed to a loss of entropy. We found that the oxidative addition of a formyl C−H bond proceeded readily, and the relative free energy of transition state **9-ts** was only 7.7 kcal/mol higher than that of intermediate **8**. However, the overall activation free energy of this step was as high as 24.7 kcal/mol, as the relative free energy of intermediate **8** can be as

DOI: 10.1021/acs.joc.5b02828
J. Org. Chem. 2016, 81, 2320−2326

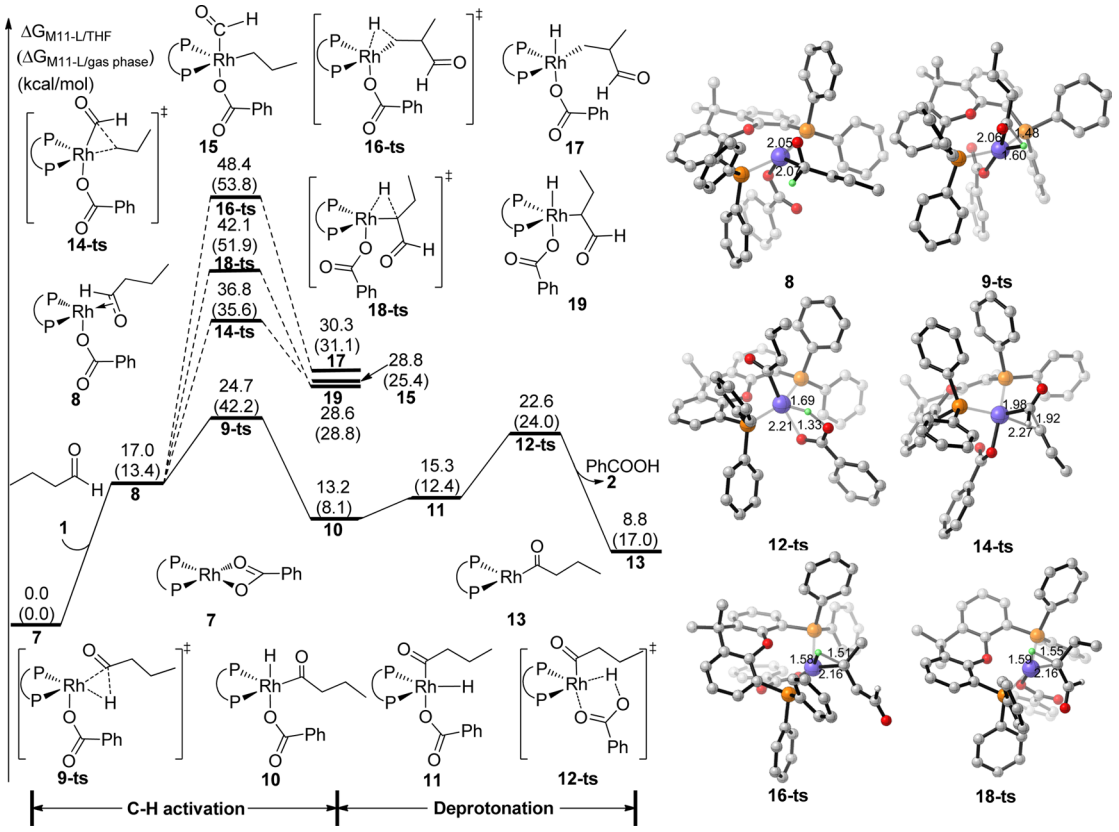

Figure 2. Free energy profiles for the initial steps of the rhodium-catalyzed transfer hydroformylation between butyraldehyde and nbd. Values are given in kcal/mol and represent the relative free energies calculated by the M11-L method in THF. The values given in parentheses are the relative free energies calculated by the M11-L method in the gas phase.

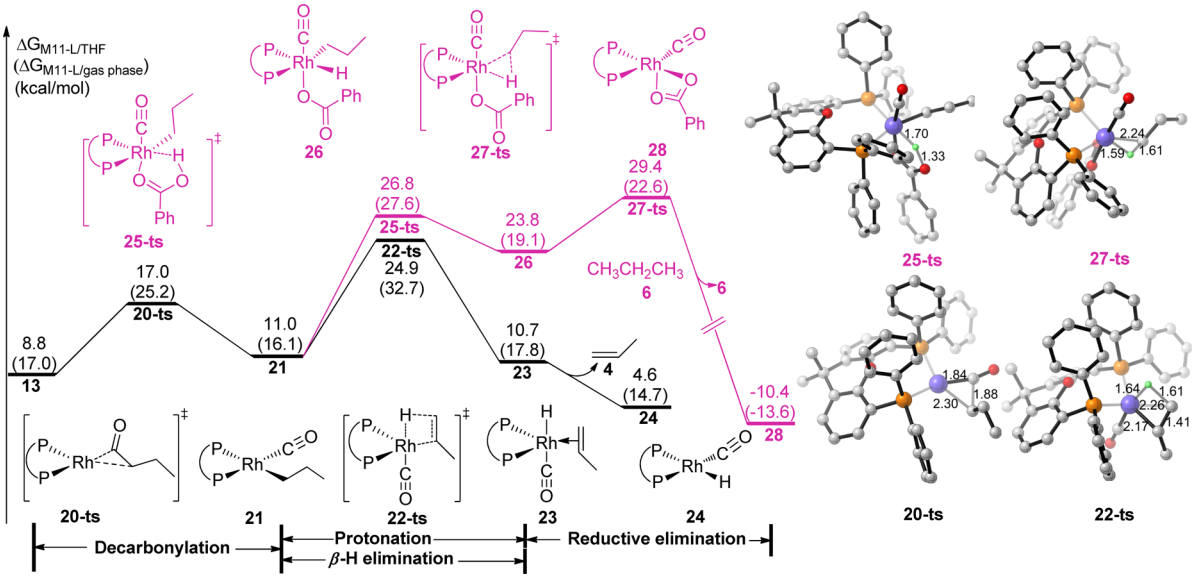

Figure 3. Free energy profiles for the olefin-releasing step of the rhodium-catalyzed transfer hydroformylation between butyraldehyde and nbd. Values are given in kcal/mol and represent the relative free energies calculated by the M11-L method in THF. The values given in parentheses are the relative free energies calculated by the M11-L method in the gas phase.

high as 17.0 kcal/mol. After the direct C−H bond oxidative addition, Rh(III) hydride intermediate **10** was formed reversibly. We also investigated the oxidative addition of the α- or β-hydrogens in butyraldehyde. However, the relative free energies of transition states **18-ts** and **16-ts** were 17.4 and 23.7 kcal/mol higher than that of transition state **9-ts**, respectively. We also studied direct C−C bond activation, but the overall activation free energy for the oxidative addition of the formyl group was as high as 36.8 kcal/mol via transition state **14-ts**. Therefore, this pathway can also be ruled out, and the transfer hydroformylation began from the oxidative addition of the formyl C−H bond. Intermediate **11** was formed by reversible

DOI: 10.1021/acs.joc.5b02828
J. Org. Chem. 2016, 81, 2320−2326

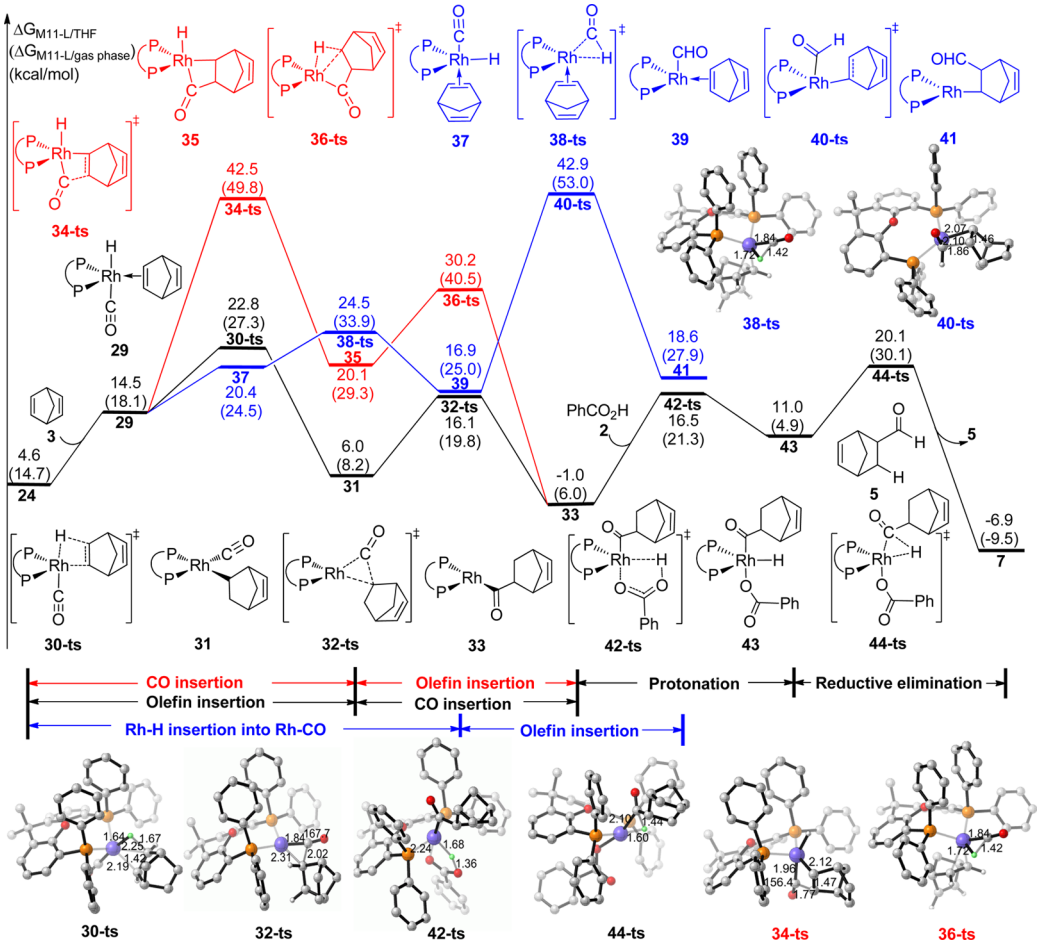

Figure 4. Free energy profiles for the nbd hydroformylation step of the rhodium-catalyzed transfer hydroformylation between butyraldehyde and nbd. Values are given in kcal/mol and represent the relative free energies calculated by the M11-L method in THF. The values given in parentheses are the relative free energies calculated by the M11-L method in the gas phase.

isomerization of intermediate **10**. The configuration of intermediate **11** was also trigonal bipyramidal, but the hydride was closer to the benzoate group. Subsequent reductive elimination then occurred via transition state **12-ts**, with a barrier of only 9.4 kcal/mol. After one molecule of benzoic acid was released, acylrhodium(I) intermediate **13** was formed.

As shown in Figure 3, when acylrhodium(I) intermediate **13** was formed, subsequent decarbonylation occurred via transition state **20-ts**, with a barrier of only 8.2 kcal/mol, to reversibly afford alkylrhodium **21**. The subsequent β-hydride elimination took place via transition state **22-ts** to form olefin-coordinated rhodium intermediate **23**. The relative free energy of that transition state was 24.9 kcal/mol, which was the highest point around the whole free energy surface. Therefore, the β-hydride elimination was the rate-determining step of the catalytic cycle. After one molecule of propene was released, rhodium hydride intermediate **24** was formed. Interestingly, the relative free energies for all the intermediates and transition states before the formation of intermediate **24** were greater than zero, meaning that all of these steps were reversible and difficult to observe experimentally. We also considered an alternative pathway that would yield propane **6** by protonation and reductive elimination. As shown in Figure 3 (pink lines), intermediate **21** was protonated by benzoic acid via transition state **25-ts**, with a barrier of 15.8 kcal/mol, to afford rhodium(III) hydride intermediate **26**. Subsequent reductive elimination via transition state **27-ts** then afforded propane **6** exothermically. As a comparison, the relative free energy of transition state **27-ts** was 4.5 kcal/mol higher than that of transition state **22-ts**; therefore, generating propane **6** was unfavorable kinetically, although this process was more exothermic.

The coordination of nbd **3** with intermediate **24** afforded intermediate **29** with a 9.9 kcal/mol endotherm because of the steric hindrance of nbd (Figure 4). The following nbd insertion into the Rh−H bond took place via transition state **30-ts** to generate an alkylrhodium intermediate **31**. After this step, subsequent carbonyl insertion occurred rapidly via transition state **32-ts**, with a barrier of only 10.1 kcal/mol, to afford an acylrhodium intermediate **33**. This was then protonated by benzoic acid via transition state **42-ts** to endothermically form rhodium hydride intermediate **43**. The final reductive elimination occurred via transition state **44-ts** to give aldehyde product **5**, and the active catalyst **7** was regenerated to complete the catalytic cycle. The formation of aldehyde **5** was exothermic by 6.9 kcal/mol, which was the driving force for the whole catalytic cycle. We also considered the order of the insertion steps for the hydroformylation of nbd. As shown in Figure 4 (red lines), when intermediate **29** was formed by the coordination of Rh to nbd, carbonyl insertion took place via transition state **34-ts** to afford four-membered ring intermediate **35**. After C−H bond reductive elimination via transition state

DOI: 10.1021/acs.joc.5b02828
J. Org. Chem. 2016, 81, 2320−2326

36-ts, the same intermediate **33** could also be formed by this pathway. However, the relative free energy of transition state **34-ts** was as high as 42.5 kcal/mol; therefore, this pathway can be ruled out.

Moreover, we performed calculations for another side pathway, which forms formyl rhodium intermediate **39** first. As shown in Figure 4 (blue lines), the relative free energy for the carbonyl insertion into the Rh−H bond to give transition state **38-ts** was only 1.7 kcal/mol higher than that for transition state **30-ts**. However, the relative free energy for transition state **40-ts** of the following nbd insertion step was as high as 42.9 kcal/mol; therefore, this pathway can also be ruled out. The DFT calculations indicated that the nbd hydroformylation involved nbd insertion into the Rh−H bond, carbonyl insertion, protonation of rhodium, and a final reductive elimination. We found the rate-limiting step of the catalytic pathway to be the β-hydride elimination, with the highest relative free energy of 24.9 kcal/mol, which was just 0.2 kcal/mol higher than that of transition state **9-ts**. The computational results showed that the hydrogen atom of the formyl group in product **5** came from the formyl group of reactant **1** and was transmitted by benzoic acid. This result coincides with experimental observations.[9]

Both the experimental and theoretical studies revealed that the counterion effect was important for this rhodium-catalyzed transfer hydroformylation. In the DFT calculations, the rhodium hydride intermediate was first deprotonated by the counterion, and the rhodium intermediate was protonated by its conjugate acid over several subsequent steps. Therefore, the alkalinity of the counterion controlled the reactivity of the deprotonation and the protonation steps.

As shown in Figure 5, when benzoate was used as the counterion, the energy barrier for the deprotonation step via

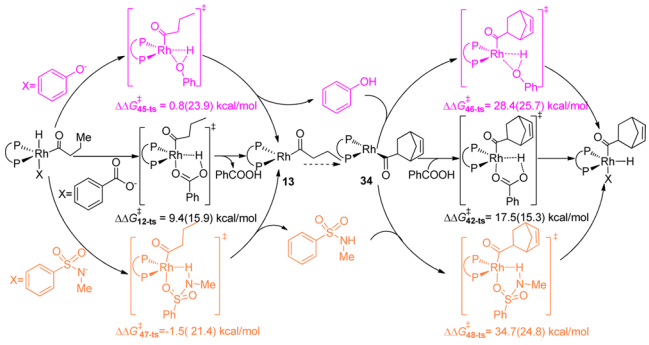

Figure 5. Counterion effect for the rhodium-catalyzed transfer hydroformylation. Values are given in kcal/mol and represent the relative free energies calculated by the M11-L method in THF. The values given in parentheses are the relative free energies calculated by the M11-L method in gas phase.

transition state **12-ts** was 9.4 kcal/mol, and for the corresponding protonation step via transition state **42-ts**, it was 17.5 kcal/mol. The results indicate that both deprotonation and protonation steps occur rapidly. On the other hand, when phenolate or sulfonylamide was used as an alternative counterion, the energy barrier for the protonation step was much higher than that with benzoate.

To clarify the counterion effect for this reaction, we calculated the electron-static potential map and nature population analysis (NPA) charge for the conjugate acid benzoic acid, phenol, and sulfonamide (Figure 6). The NPA charge clearly showed that the charge of the hydrogen atom in

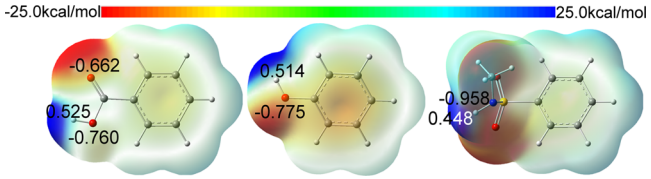

Figure 6. Electron-static potential map and nature population analysis charge for the counterions.

benzoic acid was more positive than that in phenol or sulfonamide. Therefore, the protonated ability of benzoic acid was higher than the other two conjugate acids. The computational results showed that, if phenolate or sulfonylamide was used as the counterion, the protonation step would be changed to the rate limit. Indeed, carboxylic acids would be suitable for this type of reaction.

According to our theoretical investigations into the mechanism of the rhodium-catalyzed transfer hydroformylation between butyraldehyde and nbd, we discovered that the driving force was a 6.9 kcal/mol exotherm. We also wanted to know whether the other formyl acceptors would work in this reaction. As shown in Figure 7, cyclopropene **49** was selected as a formyl acceptor to theoretically study the reactivity for the hydroformylation step. Rhodium hydride **24** was the common intermediate for the hydroformylation step and can coordinate with cyclopropene to afford intermediate **50** with a 1.0 kcal/mol exotherm. The relative free energy of intermediate **50** was 10.9 kcal/mol lower than that of intermediate **29**, which can be attributed to lower steric hindrance and more strain in the cyclopropene. The relative free energy of the following double bond insertion transition state **51-ts** was only 12.4 kcal/mol, which was also much lower than that of the nbd insertion step. Cyclopropylrhodium intermediate **52** was formed exothermically after cyclopropene insertion into the Rh−H bond. Subsequently, carbonyl insertion took place via transition state **53-ts**, with a barrier of only 6.4 kcal/mol, and afforded a cyclopropanecarbonylrhodium intermediate **54** exothermically. The protonation of rhodium by benzoic acid followed by reductive elimination released one molecule of cyclopropanecarbaldehyde and regenerated the active catalyst **7**. The computational results showed that the overall reaction was exothermic by 25.3 kcal/mol and indicated that the transfer hydroformylation between butyraldehyde and cyclopropene was thermodynamically irreversible, and the aldehyde reactant also would be fully converted to product. However, the rate limit was not involved in the half-catalytic cycle of hydroformylation; therefore, the employment of cyclopropene could not increase the reaction rate.

On the basis of our theoretical studies, the transfer hydroformylation was an equilibrium reaction, which favored generation of the more stable aldehyde and olefin. We therefore also studied the driving force of the transfer hydroformylation with selected formyl acceptors. The energy changes (ΔH_{CHO} and ΔG_{CHO}) of the transfer hydroformylation between aldehyde **59** and some selected formyl acceptors to generate olefin **60** and the corresponding aldehyde (reaction 5) are shown in Table 1.

The computational results show that when nbd or benzonorbornadiene (bnbd) were used as formyl acceptors, the reaction free energy was −9.8 or −7.6 kcal/mol, respectively, and the formyl group could completely transfer to the acceptor. However, when norbornene (nbe) was used as

DOI: 10.1021/acs.joc.5b02828
J. Org. Chem. 2016, 81, 2320−2326

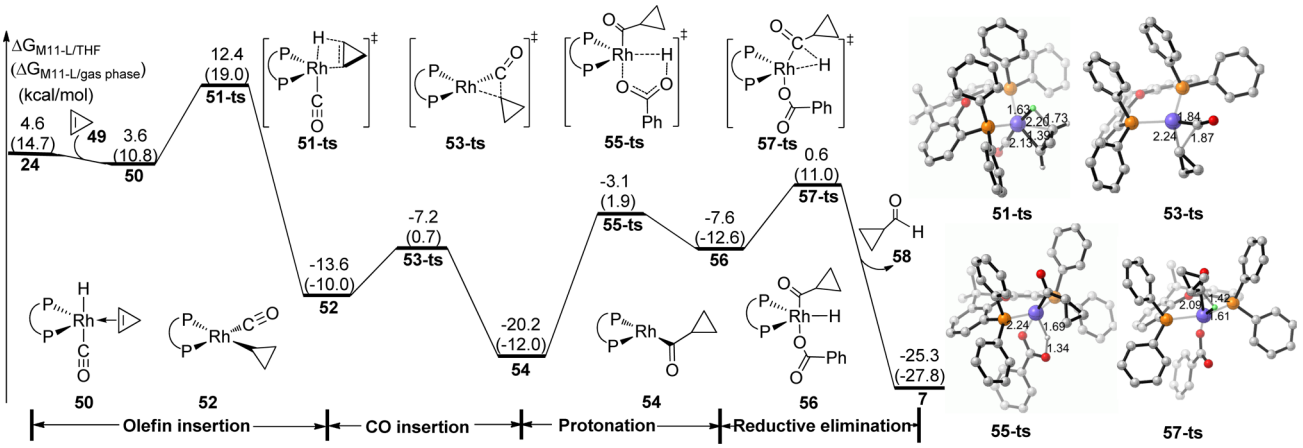

Figure 7. Free energy profiles for the rhodium-catalyzed transfer hydroformylation with cyclopropene. Values are given in kcal/mol and represent the relative free energies calculated by the M11-L method in THF. The values given in parentheses are the relative free energies calculated by the M11-L method in the gas phase.

Table 1. Reaction Free Energy and Enthalpies of Transfer Hydroformylation and Corresponding Hydrogenation of Some Selected Formyl Acceptors[a]

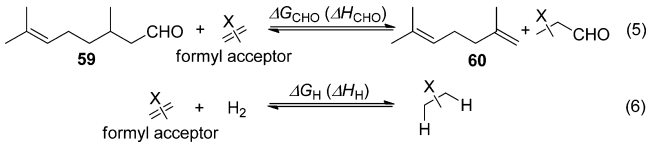

acceptor	ΔH_{CHO}	ΔG_{CHO}	ΔH_H	ΔG_H
nbd	−10.8	−9.8	−29.8	−21.0
nbe	−3.5	−2.9	−27.3	−18.6
bnbd	−8.5	−7.6	−31.2	−22.5
cyclopropene	−29.3	−28.1	−49.6	−40.5
cyclobutene	−4.7	−4.2	−27.3	−17.9
cyclopentene	1.4	1.2	−21.8	−14.3
cyclohexene	−0.8	1.1	−25.2	−15.6
propene	−2.9	−2.8	−28.5	−19.4
acetylene	−22.3	−22.7	−42.3	−34.1
phenylacetylene	−23.6	−21.1	−41.3	−31.3

[a]Values are given in kcal/mol and calculated by the M11-L method in THF; nbd, norbornadiene; nbe, norbornene; bnbd, benzonorbornadiene.

a formyl acceptor, the corresponding transfer hydroformylation was only exothermic by 2.9 kcal/mol, which indicates that the conversion rate would be lower than 99% at 40 °C. These results are highly consistent with experimental observations, in which nbe gave a lower product yield.[9] We then tested some other cyclic olefins. The computational results demonstrated that the transfer hydroformylation was exothermic when ring-strained cyclopropene or cyclobutene was used. However, when cyclopentene or cyclohexene was used, the corresponding reaction was endothermic. Interestingly, we found that when an alkyne (acetylene or phenylacetylene) was used as the formyl acceptor, the transfer hydroformylation was exothermic. Therefore, we propose that alkynes could be used as formyl acceptors in this transfer hydroformylation.

We considered that the reaction energy of the transfer hydroformylation with different formyl acceptors would correlate with the stability of their unsaturated bond. Hence, we also calculated the hydrogenation energies for those formyl acceptors (Table 1, reaction 6). As shown in Figure 8, a good

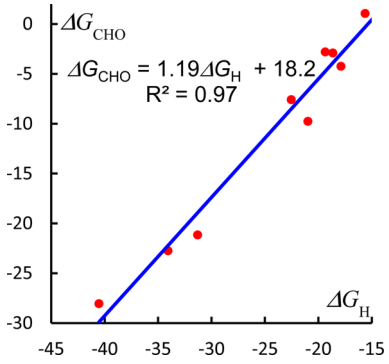

Figure 8. Relationship between the reaction free energies of transfer hydroformylation (ΔG_{CHO}) and the corresponding hydrogenation free energies (ΔG_H). Values are given in kcal/mol and represent the relative free energies calculated by the M11-L method in THF.

linear correlation was found (R^2 = 0.97). Therefore, the reaction energy of the transfer hydroformylation could be attributed to the stability of the unsaturated bond in the formyl acceptor. As an example, the hydrogenation free energy of acetylene was 34.1 kcal/mol exothermic, which was 13.1 kcal/mol higher than that of nbd. The more reactive triple bond led to a 12.9 kcal/mol more exothermic energy in the corresponding transfer hydroformylation with acetylene.

CONCLUSION

In summary, the newly reported DFT method, M11-L, has been used to establish the mechanism of the rhodium-catalyzed transfer hydroformylation reported by Dong et al. Our results show a deformylation and formylation reaction pathway. The deformylation step involves an oxidative addition of the formyl C−H bond, deprotonation with a counterion, decarbonylation, and β-hydride elimination. After olefin exchange, the formylation step takes place via an olefin insertion into the Rh−H bond, followed by a carbonyl insertion, and a final protonation with the conjugate acid of the counterion. The β-hydride elimination is found to be the rate-determining step for the whole catalytic cycle. The alkalinity of the counterion is important for this reaction. Too strong alkalinity is unfavorable for the protonation step. Therefore, a carboxylate counterion can be used in this reaction. We also found that the transfer hydroformylation is an equilibrium reaction, which favors

DOI: 10.1021/acs.joc.5b02828
J. Org. Chem. 2016, 81, 2320−2326

generation of the more stable aldehyde and olefin. The driving force for the reaction is correlated with the stability of the unsaturated bond in the formyl acceptor. Our computational results also suggest that alkynes or ring-strained olefins could be used as formyl acceptors in this reaction.

■ ASSOCIATED CONTENT

Supporting Information

The Supporting Information is available free of charge on the ACS Publications website at DOI: 10.1021/acs.joc.5b02828.

Cartesian coordinates and energies of all reported structures and full authorship of Gaussian 09 (PDF)

■ AUTHOR INFORMATION

Corresponding Authors

*E-mail: cgchen@cqu.edu.cn. Tel: +86-13608357956. Fax: +86-23-88288267.

*E-mail: lanyu@cqu.edu.cn. Tel: +86-18680805840. Fax: +86-23-88288267.

Author Contributions

§X.L. and R.B. contributed equally to this work.

Notes

The authors declare no competing financial interest.

■ ACKNOWLEDGMENTS

This project is supported by the National Science Foundation of China (Grant Nos. 21372266 and 51302327). We are also thankful for the project (No. 106112015CDJZR228806) supported by the Fundamental Research Funds for the Central Universities (Chongqing University).

■ REFERENCES

(1) (a) Wang, H.; Ren, S. B.; Zhang, J.; Zhang, W.; Liu, Y. K. *J. Org. Chem.* **2015**, *80*, 6856. (b) Tibrewal, N.; Pahari, P.; Wang, G.; Kharel, M. K.; Morris, C.; Downey, T.; Hou, Y.; Bugni, T. S.; Rohr, J. *J. Am. Chem. Soc.* **2012**, *134*, 18181. (c) He, Q.; Shyam, B.; Macounova, K.; Krtil, P.; Ramaker, D.; Mukerjee, S. *J. Am. Chem. Soc.* **2012**, *134*, 8655. (d) Hanson, S. K.; Wu, R.; Silks, L. A. *Angew. Chem., Int. Ed.* **2012**, *51*, 3410. (e) Chen, K.; Li, H.; Li, Y.; Zhang, X.-S.; Lei, Z.-Q.; Shi, Z.-J. *Chemical Science* **2012**, *3*, 1645.

(2) (a) Landis, C. R. *Science* **2015**, *347*, 29. (b) Kusumoto, S.; Tatsuki, T.; Nozaki, K. *Angew. Chem., Int. Ed.* **2015**, *54*, 8458.

(3) Lepesheva, G. I.; Waterman, M. R. *Biochim. Biophys. Acta, Gen. Subj.* **2007**, *1770*, 467.

(4) (a) Warrilow, A. G.; Hull, C. M.; Rolley, N. J.; Parker, J. E.; Nes, W. D.; Smith, S. N.; Kelly, D. E.; Kelly, S. L. *Appl. Environ. Microbiol.* **2014**, *80*, 6154. (b) Morrison, A. M.; Goldstone, J. V.; Lamb, D. C.; Kubota, A.; Lemaire, B.; Stegeman, J. J. *Biochim. Biophys. Acta, Gen. Subj.* **2014**, *1840*, 1825. (c) Waterman, M. R.; Lepesheva, G. I. *Biochem. Biophys. Res. Commun.* **2005**, *338*, 418.

(5) (a) Christensen, S. H.; Olsen, E. P.; Rosenbaum, J.; Madsen, R. *Org. Biomol. Chem.* **2015**, *13*, 938. (b) Hou, C.; Zhao, G.; Ji, Y.; Niu, Z.; Wang, D.; Li, Y. *Nano Res.* **2014**, *7*, 1364. (c) Chikkali, S. H.; van der Vlugt, J. I.; Reek, J. N. H. *Coord. Chem. Rev.* **2014**, *262*, 1. (d) Jia, X.; Wang, Z.; Xia, C.; Ding, K. *Youji Huaxue* **2013**, *33*, 1369. (e) Gadzikwa, T.; Bellini, R.; Dekker, H. L.; Reek, J. N. *J. Am. Chem. Soc.* **2012**, *134*, 2860.

(6) (a) Alagona, G.; Ghio, C. *J. Phys. Chem. A* **2015**, *119*, 5117. (b) Fristrup, P.; Kreis, M.; Palmelund, A.; Norrby, P. O.; Madsen, R. *J. Am. Chem. Soc.* **2008**, *130*, 5206. (c) Matsubara, T.; Koga, N.; Ding, Y.; Musaev, D. G.; Morokuma, K. *Organometallics* **1997**, *16*, 1065.

(7) (a) Lebold, T. P.; Wood, J. L.; Deitch, J.; Lodewyk, M. W.; Tantillo, D. J.; Sarpong, R. *Nat. Chem.* **2013**, *5*, 126. (b) Wertz, D. L.; Sisemore, M. F.; Selke, M.; Driscoll, J.; Valentine, J. S. *J. Am. Chem. Soc.* **1998**, *120*, 5331. (c) Jun, C. H.; Huh, C. W.; Na, S. J. *Angew. Chem., Int. Ed.* **1998**, *37*, 145. (d) Prince, R. H.; Raspin, K. A. *Chem. Commun.* **1966**, 156.

(8) Kondo, T.; Akazome, M.; Tsuji, Y.; Watanabe, Y. *J. Org. Chem.* **1990**, *55*, 1286.

(9) Murphy, S. K.; Park, J. W.; Cruz, F. A.; Dong, V. M. *Science* **2015**, *347*, 56.

(10) (a) Beckmann, J.; Dakternieks, D.; Duthie, A.; Lim, A. E. K.; Tiekink, E. R. T. *J. Organomet. Chem.* **2001**, *633*, 149. (b) Galli, C.; Mandolini, L. *Eur. J. Org. Chem.* **2000**, *2000*, 3117. (c) Johnson, F. *Chem. Rev.* **1968**, *68*, 375.

(11) (a) Landis, C. R. *Science* **2015**, *347*, 29. (b) Phan, D. H. T.; Kou, K. G. M.; Dong, V. M. *J. Am. Chem. Soc.* **2010**, *132*, 16354. (c) Makado, G.; Morimoto, T.; Sugimoto, Y.; Tsutsumi, K.; Kagawa, N.; Kakiuchi, K. *Adv. Synth. Catal.* **2010**, *352*, 299. (d) Lenges, C. P.; Brookhart, M. *Angew. Chem., Int. Ed.* **1999**, *38*, 3533.

(12) (a) Pirnot, M. T.; Rankic, D. A.; Martin, D. B.; MacMillan, D. W. *Science* **2013**, *339*, 1593. (b) Fu, H.; Karlsson, J.; Bylund, J.; Movitz, C.; Karlsson, A.; Dahlgren, C. *J. Leukocyte Biol.* **2006**, *79*, 247. (c) Eguillor, B.; Esteruelas, M. A.; Oliván, M.; Oñate, E. *Organometallics* **2004**, *23*, 6015. (d) Bae, Y. S.; Yi, H. J.; Lee, H. Y.; Jo, E. J.; Kim, J. I.; Lee, T. G.; Ye, R. D.; Kwak, J. Y.; Ryu, S. H. *J. Immunol.* **2003**, *171*, 6807. (e) Martinez, A. G.; Alvarez, R. M.; Barcina, J. O.; de la Moya Cerero, S.; Vilar, E. T.; Fraile, A. G.; Hanack, M.; Subramanian, L. R. *J. Chem. Soc., Chem. Commun.* **1990**, 1571.

(13) Frisch, M. J.; et al. *Gaussian 09*, revision D.01; Gaussian, Inc.: Wallingford, CT, 2013.

(14) (a) Qi, X.; Zhang, H.; Shao, A.; Zhu, L.; Xu, T.; Gao, M.; Liu, C.; Lan, Y. *ACS Catal.* **2015**, *5*, 6640. (b) Liu, D.; Tang, S.; Yi, H.; Liu, C.; Qi, X.; Lan, Y.; Lei, A. *Chem. - Eur. J.* **2014**, *20*, 15605. (c) Zhao, Y.; Ng, H. T.; Peverati, R.; Truhlar, D. G. *J. Chem. Theory Comput.* **2012**, *8*, 2824. (d) Peverati, R.; Truhlar, D. G. *Phys. Chem. Chem. Phys.* **2012**, *14*, 11363. (e) Peverati, R.; Truhlar, D. G. *J. Phys. Chem. Lett.* **2012**, *3*, 117. (f) Qi, X.; Li, Y.; Zhang, G.; Li, Y.; Lei, A.; Liu, C.; Lan, Y. *Dalton Trans.* **2015**, *44*, 11165.

(15) (a) Dolg, M.; Stoll, H.; Preuss, H. *J. Chem. Phys.* **1989**, *90*, 1730. (b) Dolg, M.; Wedig, U.; Stoll, H.; Preuss, H. *J. Chem. Phys.* **1987**, *86*, 866.

(16) (a) Roy, L. E.; Hay, P. J.; Martin, R. L. *J. Chem. Theory Comput.* **2008**, *4*, 1029. (b) Ehlers, A. W.; Böhme, M.; Dapprich, S.; Gobbi, A.; Höllwarth, A.; Jonas, V.; Köhler, K. F.; Stegmann, R.; Veldkamp, A.; Frenking, G. *Chem. Phys. Lett.* **1993**, *208*, 111. (c) Wadt, W. R.; Hay, P. J. *J. Chem. Phys.* **1985**, *82*, 284. (d) Hay, P. J.; Wadt, W. R. *J. Chem. Phys.* **1985**, *82*, 299. (e) Hay, P. J.; Wadt, W. R. *J. Chem. Phys.* **1985**, *82*, 270.

(17) Marenich, A. V.; Cramer, C. J.; Truhlar, D. G. *J. Phys. Chem. B* **2009**, *113*, 6378.

(18) Manger, M.; Wolf, J.; Teichert, M.; Stalke, D.; Werner, H. *Organometallics* **1998**, *17*, 3210.

DOI: 10.1021/acs.joc.5b02828
J. Org. Chem. 2016, 81, 2320−2326